Numerical Simulation of an Ultrasonic Vibratory Cavitation Device

Byoung Guk Kim, Philip Wilson, Stephen Turnock
Fluid Structure Interactions group, Faculty of Engineering and Environment,
University of Southampton, Southampton SO16 7QF
bgk1g15@soton.ac.uk

1 Introduction

Cavitation erosion prediction is one of the most important tasks in the ship propeller design. While predominantly qualitative methods are used such as paint tests or high speed video image analyses, there have been efforts to quantify such risks especially in the field of computational fluid dynamics (CFD).

As an experimental quantitative method to assess erosion risk, the acoustic emission (AE) technique has been employed, for example, by Lloyds Register for more than a decade now to complement their borescopic cavitation observation at the ship scale. Boorsma and Fitzsimmons (2009) reported (see Fig. 1,) its correlation with borescope observed cavitation events appeared very positive and the location of cavitation impingement on the rudder (shown in the left image of Fig. 1) coincided with the estimated location by multiple synchronous measurements of AE at different locations. If it is possible to decipher how the AE connected with the pressure waves emitted from any given cavitation event, predicting the pressure waves we may be able to predict AE and eventually where and what intensity of cavitation events occur on any given propeller or ship structures. The transfer function can be useful for establishing quantitative correlations between CFD, full-scale trial data and with model test data.

As the first step in being able to model this process and gain greater understanding in links between acoustic signal and type/location of cavitation, an open source Computational Fluid Dynamics programme openFOAM (version. 3.0.1) has been used to simulate ultrasonic cavitation on a sonotrode and hence to predict cavitation phenomena and pressure impact loads on a test specimen under the ultrasonic horn. The aim of the work is to evaluate the physical realism required and the limitations of current cavitation models.

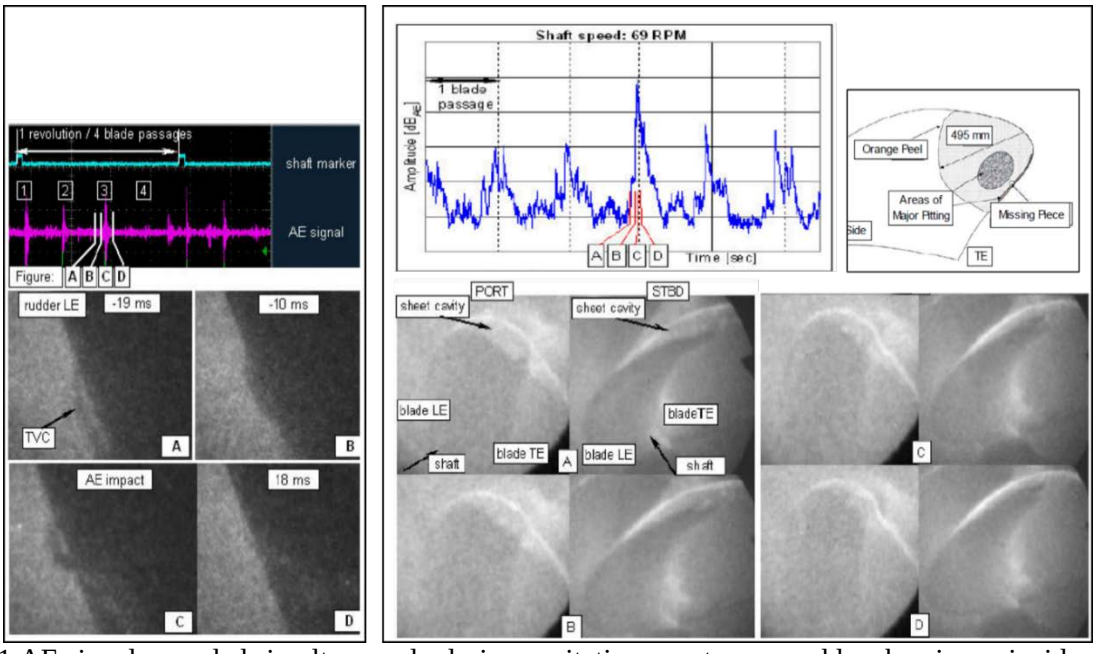

Fig. 1 AE signal recorded simultaneously during cavitation events on a rudder showing coincidence of AE burst and the tip vortex impingement moment in the image C (left) and a propeller also showing a good coincidence of AE burst and the propeller tip vortex bursting which was confirmed later by a visual inspection of the propeller (right). Boorsma and Fitzsimmons (2009).

2 Vibratory cavitation device (Sonotrode)

The device intended for the experiment is a Sonotrode. It consists of an ultrasonic transducer of which the horn tip is submerged in fresh water contained in a rectangular bath as shown in Fig. 2. Acoustic emission sensors will be placed just beneath the bottom of a rectangular test specimen. The technical specifications of the ultrasonic transducer and acoustic emission sensor as well as the approximate dimensions of the bath are described in Table 1.

Table 1 Technical specifications of the test equipment.

Sonotrode	
Manufactuer, model	Hielscher, UIP1000hd
Power output range	500 ~ 1000 W
Oscillation frequency and amplitude (peak-to-peak)	20 kHz ± 500 Hz (non-adjustable) Actual measurement results: 19.5 kHz, 43 (50 %) ~ 96 (100 %) ± 1 µm
Diameter of the ultrasonic horn	15.9 mm
Acoustic emission sensor	
Type	Ceramic-faced Piezoelectric
Frequency	150 kHz
Dimensions (mm)	20.0 x 23.7 x 10.1
Bath	
Material and shape	Transparent acrylic rectangular box
Dimensions (L x W x H, mm)	305 × 400 × 115
Liquid in the container	Fresh water at ambient temperature (5 litres)

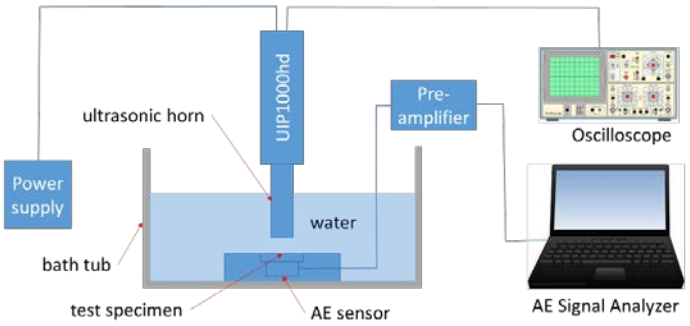

Fig. 2 Schematic instrumentation of the ultrasonic cavitation device.

3 Numerical simulation setup

There are a number of numerical validation studies on the acoustic cavitation simulation in an ultrasound field. Žnidarčič et al. (2015) reported a series of the homogeneous-mixture-based acoustic cavitation simulation results with different cavitation models. They reported failure of the conventional cavitation models in predicting the sub-harmonic oscillation of, namely the acoustic super-cavity in the ultrasound field and suggested importance of the inertia of the large cavity in describing its subharmonic oscillation in a rapidly changing pressure field. Mottyll and Skoda (2015) tried validation of their density-based compressible inviscid flow solver with barotropic cavitation model.

In this initial numerical study, to solve the unsteady Reynolds-Averaged Navier-Stokes equation, the PIMPLE (merged PISO-SIMPLE) algorithm was used together with the VoF-based Schnerr-Sauer cavitation model (in case of the two-phase simulation) and the k-ω SST (Shear Stress Transport) turbulence model as a start; the involved Reynolds number is in the order of 100 ~ 5000 suggesting laminar flow, however, considering the experimentation results of Žnidarčič et al. (2014) or Vít et al. (2014), a turbulent flow model appeared more appropriate.

An investigation was made for the flow features inside the gap between the ultrasonic horn and the test

specimen, pressure waves and the cavity development. Firstly, the solution sensitivity to the mesh size and the difference in solutions with the static mesh scheme and dynamic one were checked with an incompressible single-phase flow simulation case. The dynamic mesh scheme is to set the first cells on 'piston' and 'pistonSidewall' patches to move at a given oscillation speed of the patches. If the cells movement require re-alignment of the neighbour cells, the re-alignment is automatically done by the scheme skewing and displacing the neighbour cells. Otherwise, the size of the neighbour cells vary in the direction of the movement to compensate for the displacement of the moving cells. The flow was assumed as an incompressible single or two-phase flow to check how the pressure waves would be influenced by the development of a cavity volume.

The whole calculation domain was modelled as an axisymmetric one. The outer radius made the same as the distance from the ultrasonic horn to the shorter edge side of the rectangular bath. A schematic drawing of the model is shown in Fig. 3. The imposed boundary conditions are shown in Table 2. The simulation cases were performed for about 200 cycles (T ≈ 10 ms) based on a fixed test setup of the power setting at 50 % (peak-to-peak oscillation amplitude: 43 µm, frequency 19.5 kHz) with a fixed gap distance (= 2 mm) between the horn and the specimen.

The results of the calculation were evaluated based on the analogy of other similar published experimentation results like Žnidarčič et al. (2014) or Vít et al. (2014).

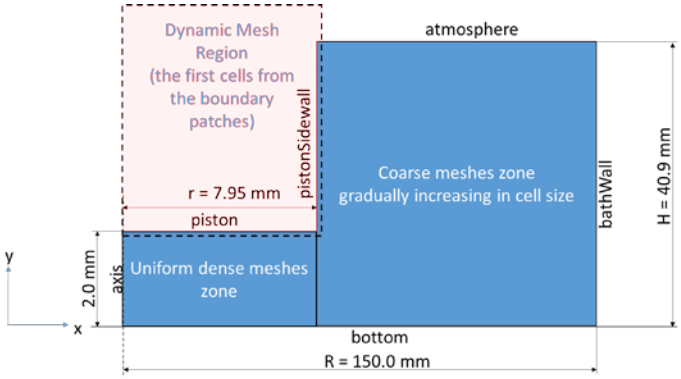

Fig. 3 Schematic drawing of the mesh.

Table 2. Finite volume boundary patches and the boundary conditions imposed on them.

Patch ID.	*p/ρ (ρ = 1000 kg/m³)*	*U*
piston & pistonSidewall	$\nabla p \cdot \vec{n} = 0$	$U_n = 2.634 * \sin(2\pi f * t)$ *where, f = 19500.*
bottom	$\nabla p \cdot \vec{n} = 0$	$\nabla \vec{U} \cdot \vec{n} = 0,$ $\nabla \vec{U} \cdot \vec{\imath} = 0$
axis	empty	empty
atmosphere	p/ρ = 101.3	$\nabla \varphi \cdot \vec{n} = \overrightarrow{U_n} = \begin{cases} \nabla \varphi \cdot \vec{n}, & \vec{n} < 0 \\ 0, & \vec{n} > 0 \end{cases}$
bathWall	p/ρ = 101.3	$\nabla \varphi \cdot \vec{n} = \overrightarrow{U_n} = \begin{cases} \nabla \varphi \cdot \vec{n}, & \vec{n} < 0 \\ 0, & \vec{n} > 0 \end{cases}$

4 Results

The initial mesh sensitivity check with the static mesh scheme and five different mesh sizes of 530, 177, 106, 76 and 59 µm (total number of cells 3000, 11000, 17000, 36400 and 54400 respectively) showed all similar streamline patterns per cycle, pressure and velocity amplitudes and tendencies. Therefore, the solution appeared rather insensitive to the mesh resolution.

The mesh scheme appears to have an influence on the flow feature inside the gap between the ultrasonic horn and the bottom where a test specimen would be placed; while the predicted pressure amplitude and frequency was almost the same as each other, the size and location of the recirculating flow structure was different from each other as shown in Fig. 4. While the static mesh scheme predicted rather a consistent inward flow along the ultrasonic horn surface and therefore a large re-circulating structure residing inside the most of the gap space, the dynamic one predicted a smaller re-circulation flow moving up and down subject to the movement of the ultrasonic horn at near the throat of the gap between the horn and the bottom.

For the single-phase non-cavitating flow case, the pressure was oscillating with a single amplitude in the order of 4.5 MPa at the driving frequency of 19.5 kHz. Reality of such a high negative pressure was in question and a short investigation was made which will be discussed in the next section.

The interchangeable two-phase (cavitating) flow case showed the sub-harmonic cavity fluctuation at a half the excitation frequency. The pressure peaks fluctuated in between 0 and 3.5 MPa at every two cycles. This is shown in Fig. 6 and Fig. 7. The typical pressure peak occurrence and corresponding cavity during the sub-harmonic oscillation period is shown in Fig. 5. The produced cavity appeared very thin. An interesting observation was that there were two travelling vortices in opposite directions each other varying at the same sub-harmonic frequency as the cavity. The vortices appear to confine the boundaries of cavities as they move along the ultrasonic horn tip surface. This may be linked to a driving mechanism of sub-harmonic cavity oscillation in addition to the inertia of the acoustic cavity as suggested by Žnidarčič et al. (2015).

The above cavitating condition simulation was repeated without the turbulence model. The results were very similar with the one with the turbulence model. Thus appears the current problem can be treated in the laminar flow regime.

5 Discussion

While there is not any available experimentation data directly comparable with the current simulation results yet, it appears to show a similar feature as found from other precedent studies, like the sub-harmonic cavity fluctuation.

Regarding the different flow feature with the static mesh scheme, although it had not been expected at first, this was thought as a result from the absence of physical displacement of the solid boundary, which in reality would have played a role of blocking the inward flow during the moving-down phase of the ultrasonic horn rather than allowing the still strong inward flow as predicted. For realistic simulation, the dynamic mesh scheme was decided to be used for the rest of study.

The presence of very strong negative pressure peaks from the single-phase incompressible flow simulation was also in question. To investigate possible cause(s), several more calculations were performed with different boundary conditions; (1) change of ‘bathWall’ patch boundary condition from the far field to a wall, (2) change of the solver to incorporate free surface and gravity. The first case did not have any noticeable influence, which confirms the wall boundary of the current calculation domain can be regarded as the far field. Consideration of the free surface had a significant influence on the pressure peak prediction. The peak was reduced to about 2.9 MPa. However, still the amplitude was thought as too high to be realistic. Finally, the atmosphere patch was forced to oscillate in the vertical direction in accordance to the mass flux through the patch, which was calculated from the volume displacement by the ultrasonic horn movement. In that case, the oscillating pressure amplitude was reduced to the order of 20 % of the given internal pressure (atmospheric pressure) in the fluid domain. The reason of the high negative pressure is thought because of incompressibility of the fluid whereas the outlet (‘atmosphere’ patch) did not allow the fluid to be displaced accordingly.

Finally, observation of the travelling vortices is discussed. As shown in the sequence of images in Fig. 7, they seemed to confine the boundaries of cavities on the surface of the ultrasonic horn tip. Furthermore,

the frequency of such travelling vortices coincided with the sub-harmonic frequency of the cavitation. Therefore, although it is not clear enough yet if this is driving mechanism of the sub-harmonic oscillation of the acoustic super-cavity, it appears they are relevant with the phenomenon at least.

6 Conclusion

In spite of not being able to be supported by any directly comparable experimentation data yet, it appears to show some of important features like the sub-harmonic cavity fluctuation as reported by many other researchers.

There was a finding that may be relevant to a driving mechanism of the sub-harmonic cavity osciallation. It looks clear the travelling vortices behave at the same sub-harmonic frequency as the ultrasound cavitation and have a relevant link with the phenomenon.

Acknowledgements

This work is being performed as a part of a joint research among Lloyds Register, SSPA Sweden AB and DSME to establish a quantitative prediction method for cavitation erosion. Our deep appreciation for their consistent support goes to them and to our colleague, Mr. Artur Lidtke, who willingly shared his experiences with openFOAM and took his time to discuss and give advice.

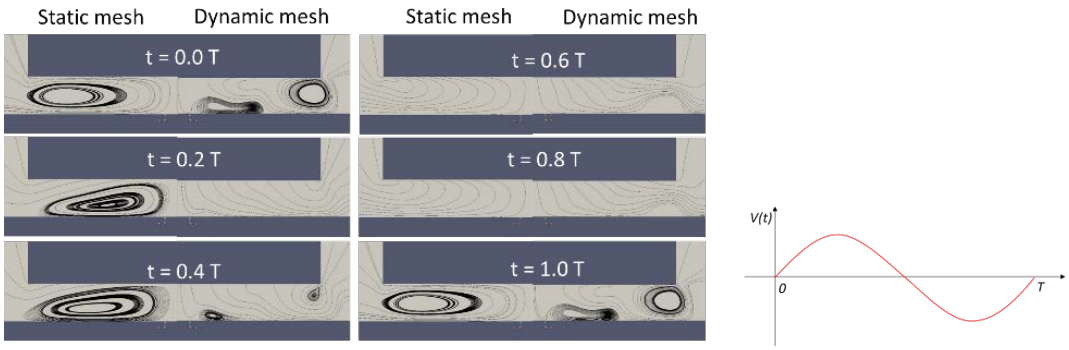

Fig. 4 Streamlines calculated with static and dynamic mesh schemes.

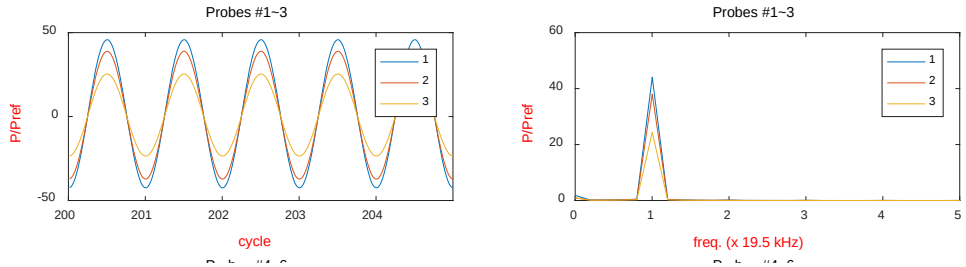

Fig. 5 Sampled time history of pressure pulses (left) and pressure harmonic analysis results (right) for an incompressible single phase flow. Probes #1~3 were located on the bottom of the gap from inside to outer edge of the gap with even spacing. The harmonic analysis results show the pressure peaks occur exactly at the same driving frequency of 19.5 kHz in the case of single-phase incompressible flow.

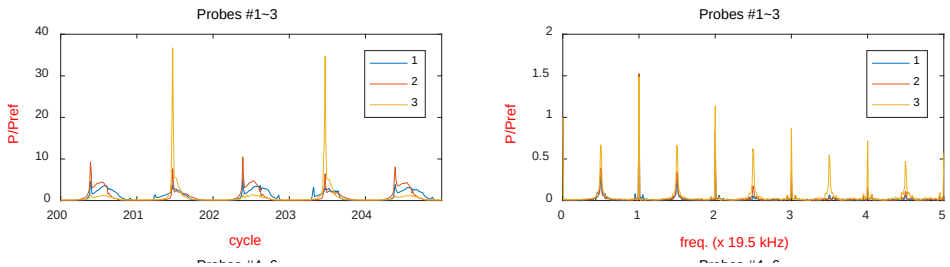

Fig. 6 Sampled time history of pressure pulses (left) and pressure harmonic analysis results (right), which shows strong power leakage over broad range of frequencies and subharmonic pulses at the frequencies corresponding to (n+1)/2 times the driving frequency (n = 0, 1, 2,...).

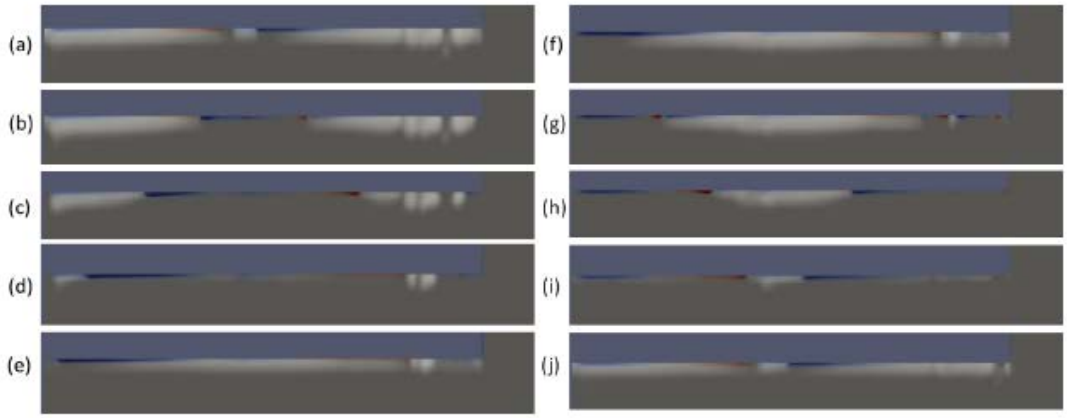

Fig. 7 Sequence of images of VoF and travelling vorticities at 0.2T interval for one sub-harmonic cycle from (a) to (j) (equivalent to the two cycles of the ultrasonic horn tip oscillation in this case). The bluish purple area shows the solid boundary of the ultrasonic horn tip and the grey part of the images show water-filled area. Travelling vortices appear to push the boundaries of cavities as they move along the surface of the ultrasonic horn tip.

References

A. Boorsma, & P. Fitzsimmons. (2009). *Quantification of Cavitation Impacts with Acoustic Emissions Techniques.*7th International Symposium on Cavitation, Ann Arbor, Michigan, USA.

S. Mottyll, & R. Skoda. (2015). Numerical 3D flow simulation of attached cavitation structures at ultrasonic horn tips and statistical evaluation of flow aggressiveness via load collectives. *Journal of Physics: Conference Series, 656*, 012052.

S. Müller, M. Fischper, S. Mottyll, R. Skoda, & J. Hussong. (2013). *Experimental investigation of the cavitating flow induced by an ultrasonic horn*.

T. Vít, S. Mottyll, S. Müller, P. Niederhofer, J. Hussong, S. Huth, . . . P. Novotný. (2014). Analysis of the cavitating flow induced by an ultrasonic horn – Numerical 3D simulation for the analysis of vapour structures and the assessment of erosion-sensitive areas. *EPJ Web of Conferences, 67*, 02078.

A. Žnidarčič, R. Mettin, C. Cairós, & M. Dular. (2014). Attached cavitation at a small diameter ultrasonic horn tip. *Physics of Fluids, 26*(2), 023304.

A. Žnidarčič, R. Mettin, & M. Dular. (2015). Modeling cavitation in a rapidly changing pressure field - application to a small ultrasonic horn. *Ultrason Sonochem, 22*, 482-492.